Journal of Solid State Chemistry **156,** 506–511 (2001)
doi:10.1006/jssc.2000.9029, available online at http://www.idealibrary.com on IDEAL®

# The Al–Li–Si System

## 2. Experimental Study and Thermodynamic Calculation of the Polythermal Equilibria

J. Gröbner, D. Kevorkov, and R. Schmid-Fetzer

*Technical University of Clausthal, Institute of Metallurgy, Robert-Koch-Strasse 42 D-38678 Clausthal-Zellerfeld, Germany*

Received October 23, 2000; accepted November 6, 2000

**The ternary Al–Li–Si system was investigated experimentally by differential thermal analysis (DTA). Melting temperatures were established for the three ternary phases, LiAlSi ($\tau_1$), $Li_{5.3}Al_{0.7}Si_2$ ($\tau_2$), and $Li_8Al_3Si_5$ ($\tau_3$), found in part 1 of this work. Additionally selected ternary alloys were also studied by DTA. These results were combined with the phase relations examined in the first part of this work. Using all these data together with the available information from the literature the ternary phase diagram was calculated applying the Calphad method. Calculated invariant reactions and isothermal sections were compared with the experimental data. The stability of the phases depending on temperature is shown using various isothermal sections and the liquidus surface. The interpretation of experimental data concerning the results of the calculation is discussed.** © 2001 Academic Press

### 1. INTRODUCTION

In the first part of this work (1) the subsolidus phase relations at 250°C were investigated. A new ternary phase $Li_8Al_3Si_5$ ($\tau_3$) was established. It crystallizes in a new structure type (Pearson symbol cP16) with a unit cell of 16 atoms. Two ternary phases LiAlSi ($\tau_1$) and $Li_{5.3}Al_{0.7}Si_2$ ($\tau_2$), which were reported in literature before (2–5), were confirmed. All phases show very little deviation from their stoichiometric composition. To understand the temperature dependence of these phase relations and the equilibria with the liquid, further investigations were made using differential thermal analysis (DTA). The obtained polythermal data together with the subsolidus phase relations enable thermodynamic optimization of the whole system after the CALPHAD method. This thermodynamic calculation was started already to select the experimental samples and was continued parallel the experimental investigations. Doing so, it was possible to focus the experimental investigations and to improve the thermodynamic calculation by an iterative feedback.

### 2. EXPERIMENTAL INVESTIGATION

#### *2.1. Methods*

For the examination of the liquidus temperatures of the system two series of alloys were investigated by thermal analysis. Starting materials were aluminum powder (99.8 mass%, Alfa), lithium bulk material (99.9 mass.%, Chemetall, Frankfurt), and silicon chips (99.9998 mass%, Wacker). The elements were weighed and mixed in glove-box with Ar atmosphere and pressed under a pressure of 100 MPa into small pellets of around 0.5 g. All alloys were prepared by levitation melting. Heating was controlled carefully to avoid evaporation. Weight loss was found less than 1 mass%. Repeating the melting of Si-rich alloys was not possible because of the absence of electric conductivity for these alloys. However, homogenization of the alloys was sufficient in all alloys due to the rapid formation of the compounds as detailed in part 1 (1). The first series of samples was made using $Al_2O_3$ crucibles. Because of evaporation, sealed Ta crucibles were used for the following series.

The samples were sealed under pure argon at 1 bar in especially adapted tantalum containers using electric arc welding. Doing so it was possible to avoid evaporation and oxidation of the samples totally. These DTA-sized containers with 8 mm diameter and 12 mm height are prepared with a highly reproducible weight (empty) of $1.23 \pm 0.03$ g, including the tantalum lid. Typical sample weights are 0.5 g. As reference, $Al_2O_3$ in another Ta crucible was used. Differential thermal analysis was performed using a Netzsch DTA 404. The heating and cooling rates were 1 K/min. No reactions with the crucibles were observed. For all samples several heating and cooling runs were performed. The temperature difference of the observed signals and the signal shift after repeated runs were below 4 K. Onset of signals was used for nonvariant reactions (heating and cooling) and for phase field boundaries on cooling. Peak maximum was used for phase field boundaries on heating. After thermal analysis the alloys were examined by X-ray powder diffractometer Siemens



0022-4596/01 $35.00

**TABLE 1**
**DTA Measurements and Calculated Thermal Signals**

| Sample composition | | DTA | Calculated | Phase field boundary |
|---|---|---|---|---|
| at. % Li | at. % Si | Thermal signal [°C][a] | Thermal arrest [°C] | and nonvariant reactions[b] |
| | | $Al_2O_3$ crucible | | |
| 41.5 | 28.6 | 818 | 825 | $L/L + \tau_3$ |
| | | 803 | 804 | $L + \tau_3/L + \tau_3 + \tau_1$ |
| | | 580 | 591 | $U_6$: $\tau_3 + (Al) = AlLi + \tau_1$[c] |
| 47.7 | 30.3 | Not measured | 832 | $L/L + \tau_3$ |
| | | 798 | 798 | $L + \tau_3/L + \tau_3 + \tau_1$ |
| 32.8 | 32.0 | 811 | 810 | $L/L + \tau_1$ |
| | | 627 | 626 | $L + \tau_1/L + \tau_1 + (Al)$ |
| 66.0 | 25.0 | 800 | 800 | $L/\tau_2$ |
| | | Sealed Ta crucible | | |
| 31.0 | 29.0 | 809 | 808 | $L/L + \tau_1$ |
| | | 640 | 641 | $L + \tau_1/L + \tau_1 + (Al)$ |
| | | 581 | 591 | $U_6$: $\tau_3 + (Al) = AlLi + \tau_1$[c] |
| 41.0 | 32.0 | 823 | 824 | $L/L + \tau_3$ |
| | | 806 | 809 | $e_1$: $L = \tau_1 + \tau_3$ |
| 50.0 | 31.0 | 833 | 832 | $L/L + \tau_3$ |
| | | 703 | 686 | $L + \tau_3/L + \tau_3 + LiAl$ |
| | | 586 | 591 | $U_6$: $\tau_3 + (Al) = AlLi + \tau_1$[c] |

[a]Estimated DTA error: $\pm$ 4 K.
[b]This interpretation of DTA signals is supported by XRD analysis.
[c]Instead of $U_6$ the reaction $E_2$: $L = AlLi + (Al) + \tau_3$, calculated at 596°C might also be possible.

D 5000 (Co$K\alpha$ radiation; step 0.02° of $2\theta$; time in the point, 3 s) to identify the phases present.

### 2.2. Results

Selection of the sample compositions results from the following approach. First thermal analysis measurements were carried out to determine the melting temperature of ternary compounds and the invariant temperatures near the liquidus. Therefore alloys with the composition of all in the literature presumed ternary phases were prepared. All samples were measured several times to verify the results. A preliminary thermodynamic model was then constructed and used to calculate essential phase equilibria. Additional sample compositions were selected at and nearby the compositions of ternary phases to check the temperatures of liquidus and invariant reactions between the phases. To investigate of the slope of the liquidus between $\tau_1$ and $\tau_3$ an additional alloy was measured. Alloy compositions and the results of DTA together with the calculated values and their interpretation are presented in Table 1. The isothermal section at 250°C in Fig. 1 illustrates the investigated alloy compositions. The obtained thermal arrests could be also compared with the calculated liquidus surface in Fig. 2. All three ternary phases melt congruently: $\tau_1$ at 811°C, $\tau_2$ at 793°C, and $\tau_3$ at 833°C. An invariant reaction was observed at about 580 to 588°C.

In casted alloys with a composition near the $\tau_1$ and $\tau_3$ phases, four phases, $\tau_1$, $\tau_3$, LiAl, and (Al), were found by X-ray diffraction. This metastable four-phase state gives a hint to a solid-state transition type reaction involving these four phases. In this reaction the well established equilibrium $\tau_1$ + LiAl (4, 6, 7) transforms to a $\tau_3$ + (Al) tie line at higher temperature.

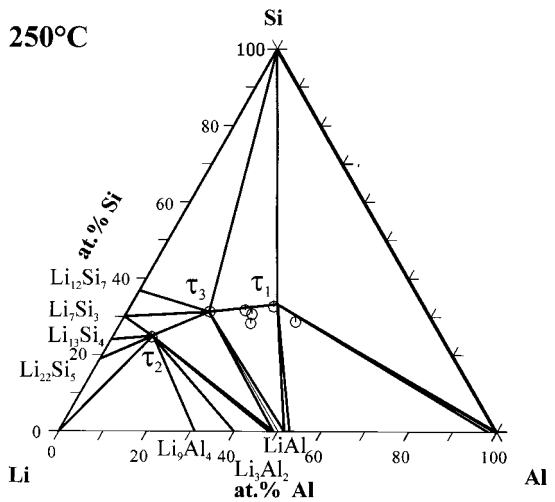


**FIG. 1.** Calculated isothermal section of Al–Li–Si phase diagram at 250°C; symbols represent the experimental compositions of samples investigated by DTA.

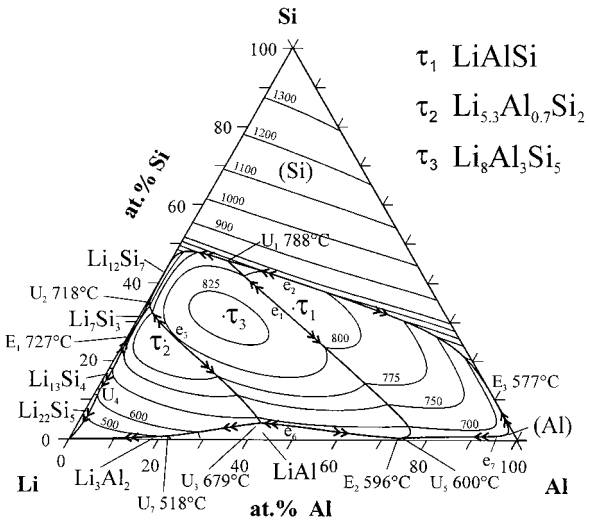


FIG. 2. Al–Li–Si phase diagram: calculated liquidus surface. Invariant reactions and fields of primary crystallization are marked.

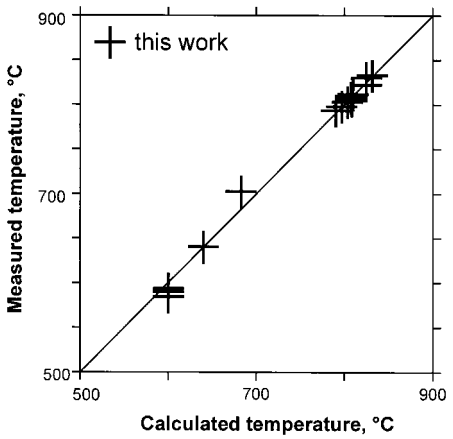


FIG. 3. Fitting between calculated and experimental DTA data.

## 3. THERMODYNAMIC MODELING

In order to calculate the ternary system by extrapolation, the thermodynamic data for the three binary subsystems are necessary. All binary data sets were available in literature. The binary Al–Si system was investigated and calculated by (8). The data set of the Al–Li was taken from the work of (9). Two data sets were published for the binary Li–Si system (10). In the first assessment of (10) the chemical potential values for the solid two-phase regions are in good agreement with the experimental values. However, the liquidus in the region of the $Li_{12}Si_7$ and $Li_7Si_3$ phases shows significant deviation to the experimental points using the same partial Gibbs energies. In the second assessment these potential values were neglected. A better agreement with the experimental phase diagram data is shown, but unrealistic values for the parameters are produced. In the present study the first assessment of (10) was preferred because of the more realistic Gibbs energies.

Using these binary data sets the ternary Al–Li–Si system was extrapolated for a preliminary calculation without considering the ternary phases. For optimization the three experimentally found (1) ternary phases, LiAlSi ($\tau_1$), $Li_{5.3}Al_{0.7}Si_2$ ($\tau_2$), and $Li_8Al_3Si_5$ ($\tau_3$), were modeled stoichiometrically by the model which is expressed by

$$G^{\tau} = x_1 G^{0,\mathrm{fcc}}_{\mathrm{Al}}(T) + x_2 G^{0,\mathrm{bcc}}_{\mathrm{Li}}(T) + x_3 G^{0,\mathrm{diamond}}_{\mathrm{Si}}(T) + \Delta_f G,$$

where $\Delta_f G$ is the Gibbs energy of formation of the stoichiometric compound referred to stable elements (Al-fcc, Li-bcc, and Si-diamond) at the temperature $T$. For the pure elements in all stable and metastable states the SGTE values published by (11) were taken, including the $H^{\mathrm{SER}}$ reference state. No homogeneity ranges were modeled since experimentally no solubilities were observed. Ternary solubilities of binary phases were also not found in our experimental investigation (1) and therefore neglected for the calculation. The liquid phase and (Al) were modeled by a simple regular solution model without any ternary interaction parameter. For the calculation the program WinPhad (12) was used.

The subsolidus phase relations found in our experimental work and the measured liquidus temperatures were used to fit Gibbs energy functions for the ternary phases. The fitting between measured and calculated temperatures from Table 1 is visually condensed in Fig. 3. All points are very close to the line for ideal agreement of experiment and calculation.

## 4. DISCUSSION

During optimization a contradiction between the higher melting temperature of $\tau_3$ (compared to $\tau_1$) and the eutectic $E_1$: $L = (\mathrm{Al}) + \mathrm{LiAl} + \tau_1$ reported by (4, 6, 7) was observed. A higher melting phase $\tau_3$ will always result in a tie line between $\tau_3$ and (Al) at higher temperature. Therefore a eutectic between (Al), LiAl, and $\tau_1$ will not occur. On the other hand, the four phases, $\tau_1$, $\tau_3$, LiAl, and (Al), found in some of our casted (not equilibrated) alloys with a composition near the $\tau_1$ and $\tau_3$ phases give a hint for an invariant reaction which may change the tie line of $\tau_3 + (\mathrm{Al})$ to $\mathrm{LiAl} + \tau_1$. In fact, in the calculation an invariant reaction $\tau_3 + (\mathrm{Al}) = \mathrm{LiAl} + \tau_1$ at 591°C emerges by fitting the parameter for $\tau_3$ and $\tau_1$ to the measured melting temperatures and the experimentally observed triangulation at 250°C. This final version of the thermodynamic data set reproduced all experimental results of the own measurements. However, the calculated liquidus surface of $\tau_1$ extends much closer to the Al corner than reported by (4) and somewhat closer than given by (6). Figure 4 illustrates the discrepancies between the different reports with dashed lines (6) and dotted lines (4) and the calculation of the partial liquidus surface with solid lines. As discussed above, a eutectic "$E_2$: $L = \mathrm{LiAl} + (\mathrm{Al}) + \tau_1$" does not take place in this calculation. However, at

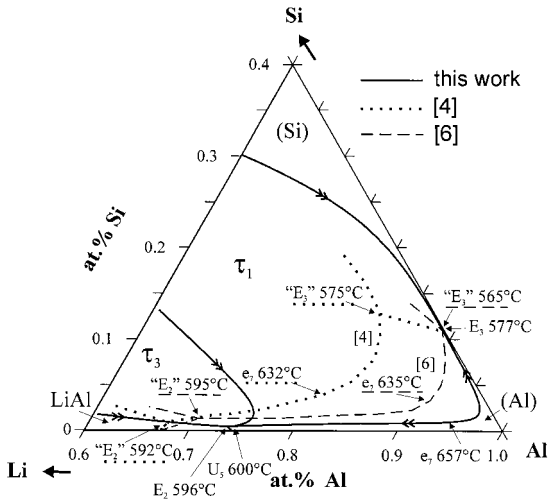


**FIG. 4.** Partial Al–Li–Si phase diagram: Liquidus surface of the Al-rich corner and isotherms. Comparison between calculation (solid lines) and the estimations after (6) (dashed) and (4) (dotted).

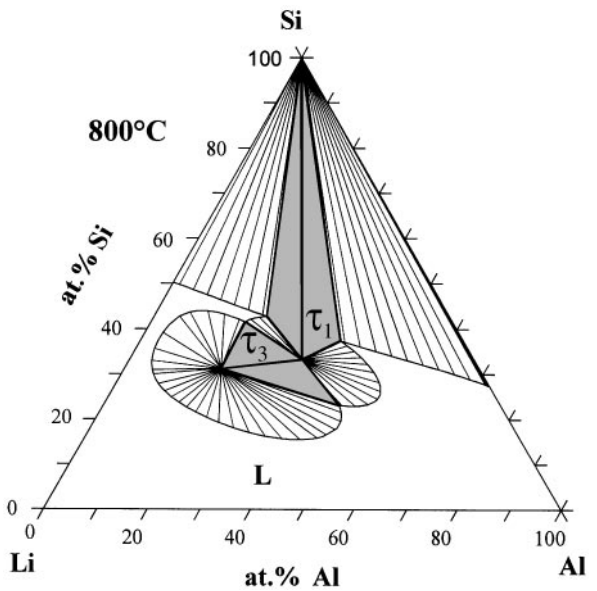


**FIG. 5.** Al–Li–Si phase diagram: calculated isothermal section at 800°C.

nearly the same temperature as given for "$E_2$" by (6) an invariant reaction, $E_2$: $L = \text{LiAl} + (\text{Al})$, $\tau_3$ is present in the calculation. It is concluded that the ternary eutectic with $\tau_3$ instead of $\tau_1$ is the correct equilibrium. The present XRD analysis also supports the calculated $E_2$ reaction, whereas no such details were given in the previous studies (4, 6, 7). In Table 2 all the invariant equilibria are given, and they compare well with the available experimental data. The integrated thermodynamic analysis of all the experimental data given the strongest support of the present interpretation.

**TABLE 2**
**Calculated Invariant Ternary Equilibria Compared with Own Measurements and Literature Data**

| | Invariant equilibrium | $T$/°C calculated | $T$/°C experimental | Experimental source |
|---|---|---|---|---|
| $e_1$ | $L = \tau_3$ | 832 | 833 | This work |
| | $L = \tau_1 + \tau_3$ | 809 | 806 | This work |
| | $L = \tau_1$ | 810 | 811 | This work |
| $e_2$ | $L = (\text{Si}) + \tau_1$ | 802 | | |
| | $L = \tau_2$ | 800 | 793 | This work |
| $e_3$ | $L = \tau_3 + \tau_2$ | 798 | | |
| $U_1$ | $L + \tau_1 = \tau_3 + (\text{Si})$ | 788 | | |
| $e_4$ | $L = \tau_2 + \text{Li}_7\text{Si}_3$ | 746 | | |
| $e_5$ | $L = \tau_2 + \text{Li}_{13}\text{Si}_4$ | 730 | | |
| $E_1$ | $L = \text{Li}_{13}\text{Si}_4 + \text{Li}_7\text{Si}_3 + \tau_2$ | 727 | | |
| $U_2$ | $L + \tau_2 = \tau_3 + \text{Li}_7\text{Si}_3$ | 718 | | |
| $e_6$ | $L = \tau_3 + \text{AlLi}$ | 686 | 703 | This work |
| $U_3$ | $L + \tau_3 = \tau_2 + \text{AlLi}$ | 679 | | |
| $e_7$ | $L = (\text{Al}) + \tau_1$ | 657 | 635 | [6] |
| | | | 632 | [4] |
| $D_1$ | $L + \text{Li}_7\text{Si}_3 = \text{Li}_{12}\text{Si}_7, \tau_3$ | 630 | | |
| $U_4$ | $L + \text{Li}_{13}\text{Si}_4 = \text{Li}_{22}\text{Si}_5 + \tau_2$ | 616 | | |
| $D_2$ | $L = (\text{Si}) + \text{Li}_{12}\text{Si}_7, \tau_3$ | 604 | | |
| $U_5$ | $L + \tau_1 = \tau_3 + (\text{Al})$ | 600 | | |
| $E_2$ | $L = \text{AlLi} + (\text{Al}) \tau_3$ | 596 | 595 | [6] |
| | | | 592 | [4] |
| $U_6$ | $\tau_3 + (\text{Al}) = \text{AlLi} + \tau_1$ | 591 | | |
| $E_3$ | $L = (\text{Al}) + (\text{Si}) + \tau_1$ | 577 | 565 | [6] |
| | | | 575 | [4] |
| $U_7$ | $L + \text{AlLi} = \text{Al}_2\text{Li}_3 + \tau_2$ | 518 | | |
| $U_8$ | $L + \text{Al}_2\text{Li}_3 = \text{Al}_4\text{Li}_9 + \tau_2$ | 334 | | |
| $D_3$ | $L = (\text{Li}) + \text{Li}_{22}\text{Si}_5, \tau_2$ | 180 | | |
| $D_4$ | $L = (\text{Li}) + \text{Al}_4\text{Li}_9, \tau_2$ | 175 | | |

The formation of the various phases are shown in several isotherms at 800 to 250°C (Figs. 5–9). At 800°C (Fig. 5) only

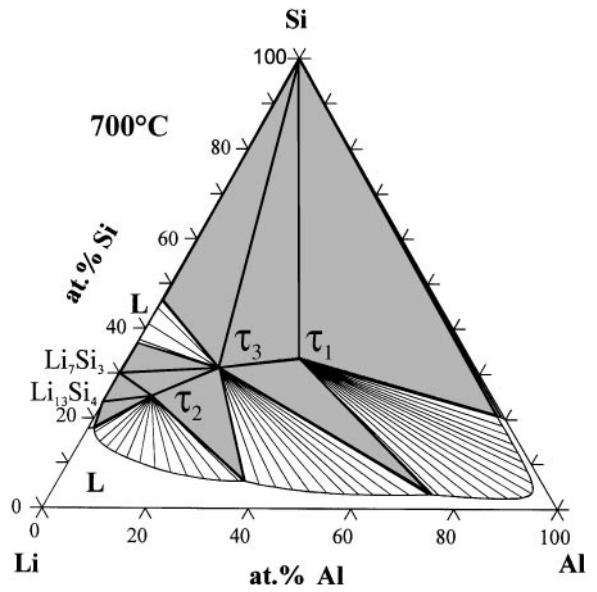


**FIG. 6.** Al–Li–Si phase diagram: calculated isothermal section at 700°C.

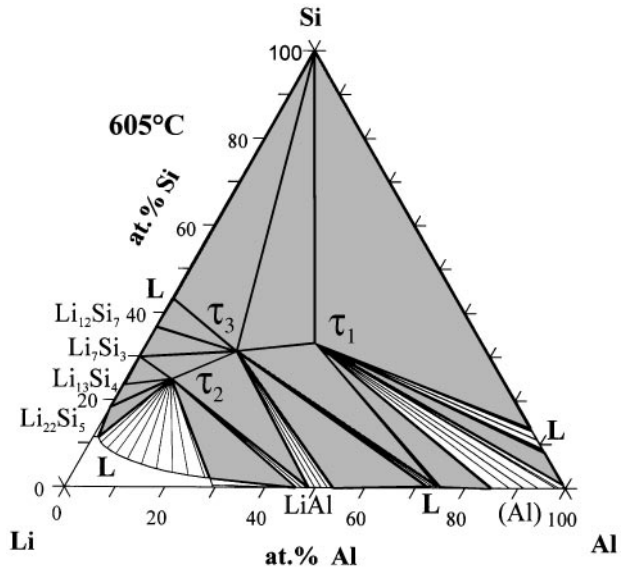


FIG. 7. Al–Li–Si phase diagram: calculated isothermal section at 605°C.

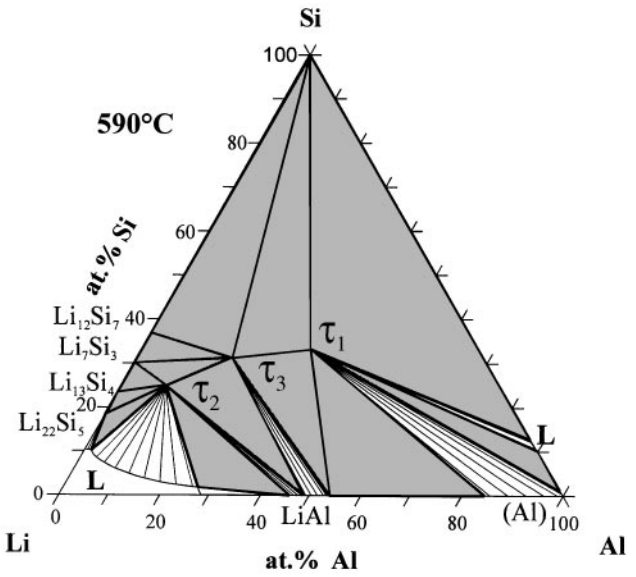


FIG. 9. Al–Li–Si phase diagram: calculated isothermal section at 590°C.

two ternary phases, $\tau_3$ and $\tau_1$, are formed. At 700°C (Fig. 6) the third ternary phase, $\tau_2$, appears together with the binary phases $Li_{13}Si_4$ and $Li_7Si_3$. Liquid phase is restricted to the whole Li–Al edge and around the binary Li–Si eutectic. At 605°C (Fig. 7) solid (Al) is in equilibrium with $\tau_1$. The need to reconcile the high melting point of $\tau_3$ with the solid state LiAl + $\tau_1$ equilibrium is resolved in a series of three nonvariant equilibria between 600 and 591°C as follows. The high melting point of $\tau_3$ gives a tie line between $\tau_3$ and an Al-rich liquid, which is also in equilibrium with $\tau_1$ in Fig. 7.

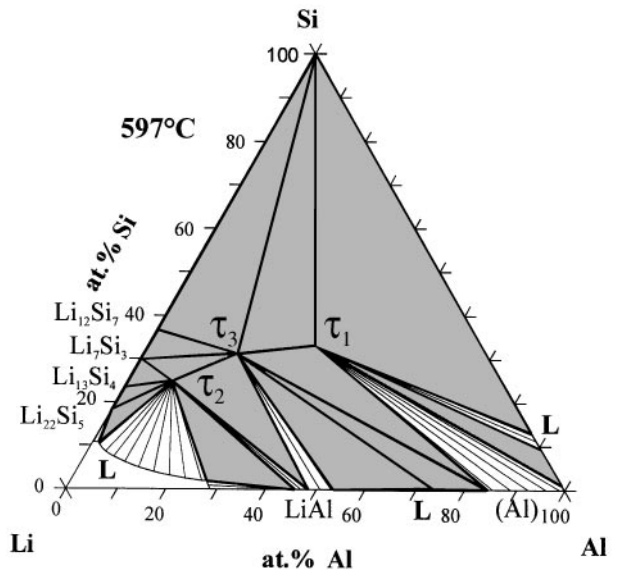


FIG. 8. Al–Li–Si phase diagram: calculated isothermal section at 597°C.

This tie line, $L + \tau_1$, transforms to a tie line between $\tau_3$ and solid (Al) in the reaction $U_5$: $L + \tau_1 = (Al) + \tau_3$ at 600°C. The result is shown in the isotherm at 597°C (Fig. 8). The heat evolution of $U_5$ is suspected to be slow, because a substantial amount of $\tau_1$ would have to be consumed in this cross-reaction. Only 4°C below, the liquid decomposes in the eutectic $E_2$ to LiAl + (Al) + $\tau_3$ at 596°C. Finally, the (Al) + $\tau_3$ equilibrium is transformed in the reaction $U_6$: $\tau_3 + (Al) = LiAl + \tau_1$ at 591°C into the $\tau_1 + LiAl$ tie line which is stable down to room temperature, as seen in Figs. 9 and 1. The reaction $U_6$ also generates the triangle $\tau_1 + LiAl + (Al)$ (Fig. 9), which is well established by literature data (4, 6, 7).

## 5. CONCLUSIONS

A consistent thermodynamic optimization of Al–Li–Si was performed and used to analyze a small number of key experiments together with literature data in the Al corner. Sample compositions for the experimental investigation were planned by preliminary calculations. The thermodynamic analysis enables a joint comparison of all DTA data—irrespective of the sample compositions—together with the phase analysis by XRD. During optimization a contradiction between a eutectic reported in literature and measured liquidus was found. All the other experimental results show excellent agreement with the calculation. Only the eutectic $E_2$: $L = LiAl + (Al) + \tau_1$ reported by (4, 6) contradicts that assessment. Our calculation proposes eutectic reaction $E_2$: $L = LiAl + (Al) + \tau_3$ as a different interpretation which is also supported by thermal analysis data.

The liquidus surface with a complete table of invariant reactions is presented. Even the solid-state four-phase reaction $\tau_3 + (Al) = LiAl + \tau_1$ is supported by nonequilibrium as-cast samples containing these four phases. The phase evolution during solidification is further illustrated by selection of calculated isothermal sections.

The ternary system Al–Li–Si is part of the development of a multicomponent database for the system Al–Ca–Li–Mg–Si. It is relevant for the design of new Mg and Al alloys. Especially in magnesium alloys, controlling the precipitation of phases from the remote Al–Li–Si system requires these well established thermodynamic data.

## ACKNOWLEDGMENTS

This work was supported by the German Research Council (DFG) in the framework of the thrust German research project SFB390 "Magnesium Technology" at the Technical University of Clausthal.

## REFERENCES

1. D. Kevorkov, J. Gröbner, and R. Schmid-Fetzer, *J. Solid State Chem.*, in press.
2. H. Nowotny and F. Holub, *Monatsh. Chem.* **91,** 877–887 (1960).
3. J. Blessing, Ph.D. thesis, Univ. Cologne, 1978.
4. M. D. Hanna and A. Hellawell, *Metall. Trans. A* **15,** 595–597 (1984).
5. V. V. Pavlyuk and O. I. Bodak, *Neorg. Mater.* **28**(5), 988–990 (1992).
6. E. S. Kadaner, V. I. Kuz'mina, and N. I. Turkina, *Russ. Metall.* (1), 150–153 (1976).
7. M. E. Drits, E. S. Kadaner, V. I. Kuz'mina, and N. I. Turkina, *Russ. Metall.* (5), 177–178 (1976).
8. J. Gröbner, H.-L. Lukas, and F. Aldinger, *CALPHAD* **20**(2), 247–254 (1996).
9. N. Saunders, *Z. Metallkd.* **80,** 894–903 (1989).
10. M. H. Braga, L. F. Malheiros, and I. Ansara, *J. Phase Equilib.* **16**(4), 324–330 (1995).
11. A. T. Dinsdale, *CALPHAD* **15,** 317 (1991).
12. "WinPhad 3.0—Phase Diagram Calculation Engine for Multicomponent Systems," CompuTherm LLC, Madison, WI 2000.